

31

Micro Heat Pipes and Micro Heat Spreaders

G. P. “Bud” Peterson
Rensselaer Polytechnic Institute

- 31.1 [Introduction](#)
Capillary Limitation • Viscous Limitation • Sonic Limitation • Entrainment Limitation • Boiling Limitation • Heat Pipe Thermal Resistance
- 31.2 [Individual Micro Heat Pipes](#)
Modeling Micro Heat Pipe Performance • Testing of Individual Micro Heat Pipes
- 31.3 [Arrays of Micro Heat Pipes](#)
Modeling of Heat Pipe Arrays • Testing of Arrays of Micro Heat Pipes • Fabrication of Arrays of Micro Heat Pipes
- 31.4 [Flat-Plate Micro Heat Spreaders](#)
Modeling of Micro Heat Spreaders • Testing of Micro Heat Spreaders • Fabrication of Micro Heat Spreaders
- 31.5 [New Designs](#)
- 31.6 [Summary and Conclusions](#)

31.1 Introduction

As described by Peterson (1994), a heat pipe operates on a closed two-phase cycle in which heat added to the evaporator region causes the working fluid to vaporize and move to the cooler condenser region, where the vapor condenses, giving up its latent heat of vaporization. In traditional heat pipes, the capillary forces existing in a wicking structure pump the liquid back to the evaporator. While the concept of utilizing a wicking structure as part of a device capable of transferring large quantities of heat with a minimal temperature drop was first introduced by Gaugler (1944), it was not until much more recently that the concept of combining phase-change heat transfer and microscale fabrication techniques (i.e., microelectromechanical systems, or MEMS, devices for the dissipation and removal of heat) was first proposed by Cotter (1984). This initial introduction envisioned a series of very small “micro” heat pipes incorporated as an integral part of semiconductor devices. While no experimental results or prototype designs were presented, the term *micro heat pipe* was first defined as one “so small that the mean curvature of the liquid–vapor interface is necessarily comparable in magnitude to the reciprocal of the hydraulic radius of the total flow channel” [Babin et al., 1990]. Early proposed applications of these devices included the removal of heat from laser diodes (Mráček, 1988) and other small localized heat-generating devices [Peterson, 1988a; 1988b]; thermal control of photovoltaic cells [Peterson, 1987a; 1987b]; removal or dissipation of heat from the leading edge of hypersonic aircraft [Camarda et al., 1997]; applications involving the nonsurgical treatment of cancerous tissue through either hyper- or hypothermia [Anon., 1989; Fletcher and Peterson, 1993]; and space applications in which heat pipes are embedded in silicon radiator panels to dissipate the large amounts of waste heat generated [Badran et al., 1993].

While not all of these applications have been implemented, micro heat pipes ranging in size from 1 mm in diameter and 60 mm in length to 30 μm in diameter and 10 mm in length have been analyzed, modeled and fabricated, and the larger of these are currently commonplace in commercially available products, such as laptop computers or high-precision equipment where precise temperature control is essential. More recently, this work has been expanded to include micro heat spreaders fabricated in silicon or in new metallized polymeric materials, which can be used to produce highly conductive, flexible heat spreaders capable of dissipating extremely high heat fluxes over large areas, thereby reducing the source heat flux by several orders of magnitude.

Since the initial introduction of the micro heat pipe concept, the study of microscale heat transfer has grown enormously and has encompassed not only phase-change heat transfer, but also the entire field of heat transfer, fluid flow and, particularly for a large number of fundamental studies, thin film behavior, as described elsewhere in this book. Microscale fluid behavior and heat transfer at the microscale, along with the variations between the behavior of bulk thermophysical properties and those that exist at the micro- or nanoscale levels are all areas of considerable interest. While the division between micro- and macroscale phase-change behavior is virtually indistinguishable, in applications involving phase-change heat transfer devices, such as micro heat pipes and micro heat spreaders, it can best be described by applying the dimensionless expression developed by Babin and Peterson (1990) and described later in this chapter. This expression relates the capillary radius of the interface and the hydraulic radius of the passage and provides a good indicator of when the forces particular to the microscale begin to dominate.

A number of previous reviews have summarized the literature published prior to 1996 [Peterson and Ortega, 1990; Peterson, 1992; Peterson et al., 1996]; however, significant advances have been made over the past several years, particularly in the development of a better understanding of the thin-film behavior that governs the operation of these devices. The following review begins with a very brief overview of the early work in this area and then looks at advances made in individual micro heat pipes, arrays of micro heat pipes and more recent investigations of flat-plate microscale heat spreaders.

For heat pipes operating in steady state, there are a number of fundamental mechanisms that limit the maximum heat transfer. These have been summarized and described in a concise format (which will be summarized here) by Marto and Peterson (1988) and include the capillary wicking limit, viscous limit, sonic limit, entrainment and boiling limits. The first two of these deal with the pressure drops occurring in the liquid and vapor phases. The sonic limit results from pressure-gradient-induced vapor velocities that may result in choked vapor flow, while the entrainment limit focuses on the entrainment of liquid droplets in the vapor stream, which inhibits the return of the liquid to the evaporator and ultimately leads to dryout. Unlike these limits, which depend upon the axial transport, the boiling limit is reached when the heat flux applied in the evaporator portion is high enough that nucleate boiling occurs in the evaporator wick, creating vapor bubbles that partially block the return of fluid.

While a description of the transient operation and start-up dynamics of these devices is beyond the scope of this work, it is appropriate to include a brief description of the methods for determining the steady-state limitations. For additional information on the theory and fundamental phenomena that cause each of these limitations, readers are referred to Tien et al. (1975), Chi (1976), Dunn and Reay (1982) and Peterson (1994).

31.1.1 Capillary Limitation

The operation and performance of heat pipes are dependent on many factors, including the shape, working fluid and wick structure. The primary mechanism by which these devices operate results from the difference in the capillary pressure across the liquid–vapor interfaces in the evaporator and condenser. To operate properly, this pressure difference must exceed the sum of all the pressure losses throughout the liquid and vapor flow paths. This relationship can be expressed as:

$$\Delta P_c \geq \Delta P_+ + \Delta P_- + \Delta P_l + \Delta P_v \quad (31.1)$$

where

- ΔP_c = net capillary pressure difference.
- ΔP_+ = normal hydrostatic pressure drop.
- ΔP_- = axial hydrostatic pressure drop.
- ΔP_l = viscous pressure drop occurring in the liquid phase.
- ΔP_v = viscous pressure drop occurring in the vapor phase.

As long as this condition is met, liquid is returned to the evaporator. For situations where the summation of the viscous pressure losses, ΔP_l and ΔP_v , and the hydrostatic pressure losses, ΔP_+ and ΔP_- , is greater than the capillary pressure difference between the evaporator and condenser, the wicking structure becomes starved of liquid and dries out. This condition, referred to as the capillary wicking limitation, varies according to the wicking structure, working fluid, evaporator heat flux and operating temperature.

31.1.1.1 Capillary Pressure

The capillary pressure difference at a liquid–vapor interface, ΔP_c , is defined by the LaPlace–Young equation, which for most heat pipe applications reduces to:

$$\Delta P_{c,m} = \left(\frac{2\sigma}{r_{c,e}} \right) - \left(\frac{2\sigma}{r_{c,c}} \right) \quad (31.2)$$

where $r_{c,e}$ and $r_{c,c}$ represent the radii of curvature in the evaporator and condenser regions, respectively.

During normal heat pipe operation, the vaporization occurring in the evaporator causes the liquid meniscus to recede into the wick, reducing the local capillary radius, $r_{c,e}$, while condensation in the condenser results in increases in the local capillary radius, $r_{c,c}$. It is this difference in the two radii of curvature that “pumps” liquid from the condenser to the evaporator. During steady-state operation, it is generally assumed that the capillary radius in the condenser, $r_{c,c}$, approaches infinity, so that the maximum capillary pressure for a heat pipe operating at steady state can be expressed as a function of only the capillary radius of the evaporator wick,

$$\Delta P_{c,m} = \left(\frac{2\sigma}{r_{c,e}} \right) \quad (31.3)$$

Values for the effective capillary radius, $r_{c,e}$, can be found theoretically for simple geometries [Chi, 1976] or experimentally for other more complicated structures.

31.1.1.2 Hydrostatic Pressure Drops

The normal and axial hydrostatic pressure drops, ΔP_+ and ΔP_- , are the result of the local gravitational body force. The normal and axial hydrostatic pressure drops can be expressed as:

$$\Delta P_+ + \rho_l g d_v \cos \Psi \quad (31.4)$$

and

$$\Delta P_- = \rho_l g L \sin \Psi \quad (31.5)$$

where ρ_l is the density of the liquid, g is the gravitational acceleration, d_v is the diameter of the vapor portion of the pipe, Ψ is the angle the heat pipe makes with respect to the horizontal, and L is the length of the heat pipe.

In a gravitational environment, the axial hydrostatic pressure term may either assist or hinder the capillary pumping process depending upon whether the tilt of the heat pipe promotes or hinders the flow of liquid back to the evaporator (i.e., the evaporator lies either below or above the condenser). In a zero- g environment or for cases where the surface tension forces dominate, such as micro heat pipes, both of these terms can be neglected.

31.1.1.3 Liquid Pressure Drop

As the liquid returns from the condenser to the evaporator, it experiences a viscous pressure drop, ΔP_l , which can be written in terms of the frictional drag,

$$\frac{dP_l}{dx} = -\frac{2\tau_l}{(r_{h,l})} \quad (31.6)$$

where τ_l is the frictional shear stress at the liquid–solid interface and $r_{h,l}$ is the hydraulic radius, defined as twice the cross-sectional area divided by the wetted perimeter.

This pressure gradient is a function of the Reynolds number, Re_l , and drag coefficient, f_l , defined as:

$$Re_l = \frac{2(r_{h,l})\rho_l V_l}{\mu_l} \quad (31.7)$$

and

$$f_l = \frac{2\tau_l}{\rho_l V_l^2} \quad (31.8)$$

respectively, where V_l is the local liquid velocity which is related to the local heat flow,

$$V_l = \frac{q}{\varepsilon A_w \rho_l \lambda} \quad (31.9)$$

A_w is the wick cross-sectional area, ε is the wick porosity, and λ is the latent heat of vaporization.

Combining these expressions yields an expression for the pressure gradient in terms of the Reynolds number, drag coefficient and the thermophysical properties:

$$\frac{dP_l}{dx} = \left(\frac{(f_l Re_l) \mu_l}{2\varepsilon A_w (r_{h,l})^2 \lambda \rho_l} \right) q \quad (31.10)$$

which in turn can be written as a function of the permeability, K , as:

$$\frac{dP_l}{dx} = \left(\frac{\mu_l}{K A_w \lambda \rho_l} \right) q \quad (31.11)$$

where the permeability expressed as:

$$K = \frac{2\varepsilon (r_{h,l})^2}{f_l Re_l} \quad (31.12)$$

For steady-state operation with constant heat addition and removal, Eq. (31.11) can be integrated over the length of the heat pipe to yield:

$$\Delta P_l = \left(\frac{\mu_l}{K A_w \lambda \rho_l} \right) L_{eff} q \quad (31.13)$$

where L_{eff} is the effective heat pipe length defined as:

$$L_{eff} = 0.5 L_e + L_a + 0.5 L_c \quad (31.14)$$

31.1.1.4 Vapor Pressure Drop

The methods for calculating the vapor pressure drop in heat pipes is similar to that used for the liquid pressure drop described above but is complicated by the mass addition and removal in the evaporator and condenser, respectively, and by the compressibility of the vapor phase. As a result, accurate computation of the total pressure drop requires that the dynamic pressure be included. In-depth discussions of the methodologies for determining the overall vapor pressure drop have been presented previously by Chi (1976), Dunn and Reay (1982) and Peterson (1994). The resulting expression is similar to that developed for the liquid:

$$\Delta P_v = \left(\frac{C(f_v Re_v) \mu_v}{2(r_{h,v})^2 A_v \rho_v \lambda} \right) L_{eff} q \quad (31.15)$$

where $(r_{h,v})$ is the hydraulic radius of the vapor space and C is a constant that depends on the Mach number.

Unlike the liquid flow, which is driven by the capillary pressure difference and hence is always laminar, the vapor flow is driven by the temperature gradient and for high heat-flux applications may result in turbulent flow conditions. As a result, it is necessary to determine the vapor flow regime as a function of the heat flux by evaluating the local axial Reynolds number, defined as:

$$Re_v = \frac{2(r_{h,v})q}{A_v \mu_v \lambda} \quad (31.16)$$

Due to compressibility effects, it is also necessary to determine if the flow is compressible. This is accomplished by evaluating the local Mach number, defined as:

$$Ma_v = \left(\frac{q}{A_v \rho_v \lambda (R_v T_v \gamma_v)} \right)^{1/2} \quad (31.17)$$

where R_v is the gas constant, T_v is the vapor temperature, and γ_v is the ratio of specific heats, which is equal to 1.67, 1.4 or 1.33 for monatomic, diatomic and polyatomic vapors, respectively (Chi, 1976).

Previous investigations summarized by Kraus and Bar-Cohen (1983) have demonstrated that the following combinations of these conditions can be used with reasonable accuracy:

$$\begin{aligned} Re_v < 2300, \quad Ma_v < 0.2 \\ (f_v Re_v) &= 16 \\ C &= 1.00 \end{aligned} \quad (31.18)$$

$$\begin{aligned} Re_v < 2300, \quad Ma_v > 0.2 \\ (f_v Re_v) &= 16 \\ C &= \left[1 + \left(\frac{\gamma_v - 1}{2} \right) Ma_v^2 \right]^{-1/2} \end{aligned} \quad (31.19)$$

$$\begin{aligned} Re_v > 2300, \quad Ma_v < 0.2 \\ (f_v Re_v) &= 0.038 \left(\frac{2(r_{h,v})q}{A_v \mu_v \lambda} \right)^{3/4} \\ C &= 1.00 \end{aligned} \quad (31.20)$$

$$\begin{aligned}
Re_v &> 2300, \quad Ma_v > 0.2 \\
(f_v Re_v) &= 0.038 \left(\frac{2(r_{h,v}) q}{A_v \mu_v \lambda} \right)^{3/4} \\
C &= \left[1 + \left(\frac{\gamma_v - 1}{2} \right) Ma_v^2 \right]^{-1/2}
\end{aligned} \tag{31.21}$$

The solution procedure is to first assume laminar, incompressible flow and then to compute the Reynolds and Mach numbers. Once these values have been found, the initial assumptions of laminar, incompressible flow can be evaluated and the appropriate modifications made.

31.1.2 Viscous Limitation

At very low operating temperatures, the vapor pressure difference between the closed end of the evaporator (the high-pressure region) and the closed end of the condenser (the low-pressure region) may be extremely small. Because of this small pressure difference, the viscous forces within the vapor region may prove to be dominant and hence limit the heat pipe operation. Dunn and Reay (1982) discuss this limit in more detail and suggest the criterion:

$$\frac{\Delta P_v}{P_v} < 0.1 \tag{31.22}$$

for determining when this limit might be of a concern. For steady-state operation, or applications in the moderate operating temperature range, the viscous limitation will normally not be important.

31.1.3 Sonic Limitation

The sonic limitation in heat pipes is the result of vapor velocity variations along the length of the heat pipe due to the axial variation of the vaporization and condensation. Much like the effect of decreased outlet pressure in a converging–diverging nozzle, decreased condenser temperature results in a decrease in the evaporator temperature up to but not beyond that point where choked flow occurs in the evaporator, causing the sonic limit to be reached. Any further decreases in the condenser temperature do not reduce the evaporator temperature or the maximum heat transfer capability, due to the existence of choked flow.

The sonic limitation in heat pipes can be determined as:

$$q_{s,m} = A_v \rho_v \lambda \left(\frac{\gamma_v R_v T_v}{2(\gamma_v + 1)} \right)^{1/2} \tag{31.23}$$

where T_v is the mean vapor temperature within the heat pipe [Chi, 1976].

31.1.4 Entrainment Limitation

In an operating heat pipe, the liquid and vapor typically flow in opposite directions, resulting in a shear stress at the interface. At very high heat fluxes, liquid droplets may be picked up or entrained in the vapor flow. This entrainment results in dryout of the evaporator wick due to excess liquid accumulation in the condenser. The Weber number, We , which represents the ratio of the viscous shear force to the force resulting from the liquid surface tension, can be used to determine at what point this entrainment is likely to occur:

$$We = \frac{2(r_{h,w}) \rho_v V_v^2}{\sigma} \tag{31.24}$$

To prevent the entrainment of liquid droplets in the vapor flow, the Weber number must therefore be less than one, which implies that the maximum transport capacity based on the entrainment limitation may be determined as:

$$q_{e,m} = A_v \lambda \left(\frac{\sigma \rho_v}{2(r_{h,w})} \right)^{1/2} \quad (31.25)$$

where $(r_{h,w})$ is the hydraulic radius of the wick structure (Dunn and Reay, 1983).

31.1.5 Boiling Limitation

As mentioned, all of the limits discussed previously depend upon the axial heat transfer. The boiling limit, however, depends upon the evaporator heat flux and occurs when the nucleate boiling in the evaporator wick creates vapor bubbles that partially block the return of fluid. The presence of vapor bubbles in the wick requires both the formation of bubbles and also the subsequent growth of these bubbles. Chi (1976) has developed an expression for the boiling limit, which can be written as

$$q_{b,m} = \left(\frac{2\pi L_{eff} k_{eff} T_v}{\lambda \rho_v \ln(r_i/r_v)} \right) \left(\frac{2\sigma}{r_n} - \Delta P_{c,m} \right) \quad (31.26)$$

where k_{eff} is the effective thermal conductivity of the liquid–wick combination, r_i is the inner radius of the heat pipe wall, and r_n is the nucleation site radius [Dunn and Reay, 1982].

31.1.6 Heat Pipe Thermal Resistance

Once the maximum transport capacity is known, it is often useful to determine the temperature drop between the evaporator and condenser. The overall thermal resistance for a heat pipe is comprised of nine resistances of significantly different orders of magnitude, arranged in a series/parallel combination. These resistances can be summarized as follows:

- R_{pe} = radial resistance of the pipe wall at the evaporator.
- R_{we} = resistance of the liquid–wick combination at the evaporator.
- R_{ie} = resistance of the liquid–vapor interface at the evaporator.
- R_{ya} = resistance of the adiabatic vapor section.
- R_{pa} = axial resistance of the pipe wall.
- R_{wa} = axial resistance of the liquid–wick combination.
- R_{ic} = resistance of the liquid–vapor interface at the condenser.
- R_{wc} = resistance of the liquid–wick combination at the condenser.
- R_{pc} = radial resistance of the pipe wall at the condenser.

Previous investigations have indicated that typically the resistance of the vapor space, the axial resistances of the pipe wall and liquid–wick combinations, can all be neglected. In addition, the liquid–vapor interface resistances and the axial vapor resistance can, in most situations, be assumed to be negligible. This leaves only the pipe wall radial resistances and the liquid–wick resistances at both the evaporator and condenser.

As presented by Peterson (1994), the radial resistances at the pipe wall can be computed from Fourier's law as:

$$R_{pe} = \frac{\delta}{k_p A_e} \quad (31.27)$$

for flat plates, where δ is the plate thickness and A_e is the evaporator area, or

$$R_{pe} = \frac{\ln(d_o/d_i)}{2\pi L_e k_p} \quad (31.28)$$

for cylindrical pipes, where L_e is the evaporator length. An expression for the equivalent thermal resistance of the liquid–wick combination in circular pipes is

$$R_{we} = \frac{\ln(d_o/d_i)}{2\pi L_e k_{eff}} \quad (31.29)$$

where k_{eff} is the effective conductivity of the liquid–wick combination.

Combining these individual resistances allows the overall thermal resistance to be determined, which when combined with the maximum heat transport found previously will yield an estimation of the overall temperature drop.

31.2 Individual Micro Heat Pipes

The earliest embodiments of micro heat pipes typically consisted of a long thin tube with one or more small noncircular channels that utilized the sharp-angled corner regions as liquid arteries. While initially quite novel in size (see Figure 31.1), it was soon apparent that devices with characteristic diameters of approximately 1 mm functioned in nearly the same manner as larger, more conventional liquid artery heat pipes. Heat applied to one end of the heat pipe vaporizes the liquid in that region and forces it to move to the cooler end, where it condenses and gives up the latent heat of vaporization. This vaporization and condensation process causes the liquid–vapor interface in the liquid arteries to change continually along the pipe, as illustrated in Figure 31.2 and results in a capillary pressure difference between the evaporator and condenser regions. This capillary pressure difference promotes the flow of the working fluid from the condenser back to the evaporator through the triangular-shaped corner regions. These corner regions serve as liquid arteries, thus no wicking structure is required [Peterson, 1990; 1994]. The following sections present a summary of the analytical and experimental investigations conducted on individual micro heat pipes, arrays of micro heat pipes, flat-plate microscale heat spreaders, and the latest advances in the development of highly conductive, flexible, phase-change heat spreaders.

31.2.1 Modeling Micro Heat Pipe Performance

The first steady-state analytical models of individual micro heat pipes utilized the traditional pressure-balance approach developed for use in more conventional heat pipes and described earlier in this chapter. These models provided a mechanism by which the steady-state and transient performance characteristics of micro heat pipes could be determined and indicated that, while the operation was similar to that observed in larger more conventional heat pipes, the relative importance of many of the parameters is quite different. Perhaps the most significant difference was the relative sensitivity of the micro heat pipes

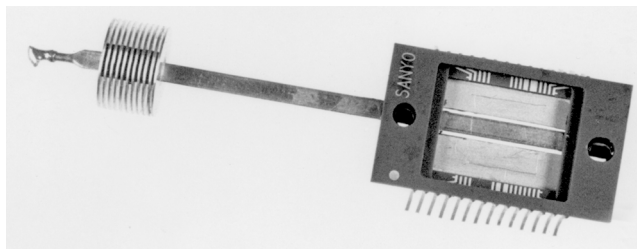


FIGURE 31.1 Micro-heat-pipe-cooled ceramic chip carrier. (From Peterson, G.P. (1994) *An Introduction to Heat Pipes: Modeling, Testing and Applications*, John Wiley & Sons, New York. With permission.)

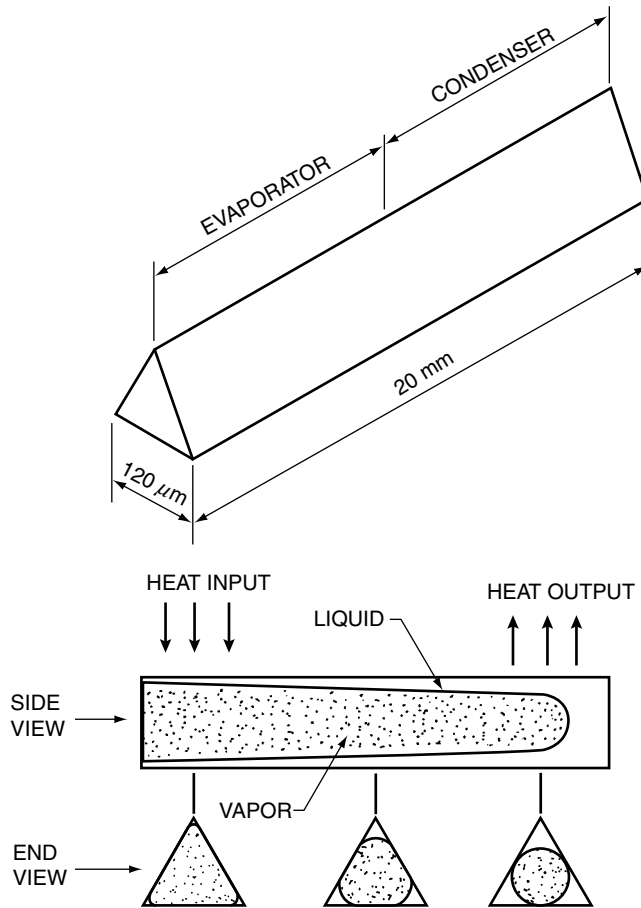


FIGURE 31.2 Micro heat pipe operation. (From Peterson, G.P. et al. (1996) in *Microscale Energy Transport* (C.L. Tien et al., Eds.), Taylor & Francis, Washington, D.C. Reproduced by permission of Routledge, Inc.)

to the amount of working fluid present. These early steady-state models later led to the development of both transient numerical models and three-dimensional numerical models of the temperature and pressure distribution within individual micro heat pipes [Peterson, 1992; 1994; Peterson et al., 1996].

31.2.1.1 Steady-State Modeling

The first steady-state model specifically designed for use in the modeling of micro heat pipes was developed by Cotter (1984). Starting with the momentum equation and assuming uniform cross-sectional area and no-slip conditions at the boundaries, this expression was solved for both the liquid and vapor pressure differentials and then combined with the continuity expression. The result was a first-order ordinary differential equation, which related the radius of curvature of the liquid–vapor interface to the axial position along the pipe. Building upon this model, Peterson (1988a) and Babin et al. (1990) developed a steady-state model for a trapezoidal micro heat pipe, using the conventional steady-state modeling techniques outlined by Chi (1976) and described earlier in this chapter. The resulting model demonstrated that the capillary pumping pressure governed the maximum heat transport capacity of these devices.

A comparison of the performance limitations resulting from the models presented by Cotter (1984) and by Babin et al. (1990) indicated significant differences in the capillary limit predicted by the two models. These differences have been analyzed and found to be the result of specific assumptions made in the initial formulation of the models [Peterson, 1992].

A comparative analysis of these two early models was performed by Gerner et al. (1992), who indicated that the most important contributions of Babin et al. (1990) were the inclusion of the gravitational body force and the recognition of the significance of the vapor pressure losses. In addition, the assumption that the pressure gradient in the liquid flow passages was similar to that occurring in Hagen–Poiseuille flow was questioned, and a new scaling argument for the liquid pressure drop was presented. In this development, it was assumed that the average film thickness was approximately one fourth the hydraulic radius, resulting in a modified expression for the capillary limitation.

A significant contribution made by Gerner et al. (1992) was the recognition that the capillary limit may never actually be reached due to Kelvin–Helmholtz-type instabilities occurring at the liquid–vapor interface. Using stability analysis criteria for countercurrent flow in tubes developed by Tien et al. (1979) and minimizing the resulting equations, the wavelength was found to be approximately 1 cm for atmospheric water and methanol. Because this length was long with respect to the characteristic wavelength, it was assumed that gravity was the dominant stabilizing mechanism. The decision as to whether to use the traditional capillary limit proposed by Babin et al. (1990) or the interfacial instability limit proposed by Gerner et al. (1992) should be governed by evaluating the shape and physical dimensions of the specific micro heat pipe being considered.

31.2.1.2 Transient Modeling

As heat pipes diminish in size, the transient nature becomes of increasing interest. The ability to respond to rapid changes in heat flux coupled with the need to maintain constant evaporator temperature in modern high-powered electronics necessitates a complete understanding of the temporal behavior of these devices. The first reported transient investigation of micro heat pipes was conducted by Wu and Peterson (1991). This initial analysis utilized the relationship developed by Collier (1981) and was used later by Colwell and Chang (1984) to determine the free-molecular-flow mass flux of evaporation. The most interesting result from this model was the observation that reverse liquid flow occurred during the startup of micro heat pipes. As explained in the original reference [Wu et al., 1991], this reverse liquid flow is the result of an imbalance in the total pressure drop and occurs because the evaporation rate does not provide an adequate change in the liquid–vapor interfacial curvature to compensate for the pressure drop. As a result, the increased pressure in the evaporator causes the meniscus to recede into the corner regions, forcing liquid out of the evaporator and into the condenser. During startup, the pressure of both the liquid and vapor is higher in the evaporator and gradually decreases with position, promoting flow away from the evaporator. Once the heat input reaches full load, the reverse liquid flow disappears and the liquid mass flow rate into the evaporator gradually increases until a steady-state condition is reached. At this time, the change in the liquid mass flow rate is equal to the change in the vapor mass flow rate for any given section [Wu and Peterson, 1991].

Several, more detailed transient models have been proposed. Badran et al. (1993) developed a conjugate model to account for the transport of heat within the heat pipe and conduction within the heat pipe case. This model indicated that the specific thermal conductivity of micro heat pipes (effective thermal conductivity divided by the density) could be as high as 200 times that of copper and 100 times that of Gr/Cu composites. Longtin et al. (1994) developed a one-dimensional, steady-state model that indicated that the maximum heat transport capacity varied with respect to the cube of the hydraulic diameter, and Khrustalev and Faghri (1994) presented a detailed mathematical model of the heat- and mass-transfer processes in micro heat pipes which described the distribution of the liquid and the thermal characteristics as a function of the liquid charge. The liquid flow in the triangular-shaped corners of a micro heat pipe with a polygonal cross section was considered by accounting for the variation of the curvature of the free liquid surface and the interfacial shear stresses due to the liquid–vapor interaction. A comparison of the predicted results with the experimental data obtained by Wu and Peterson (1991) and Wu et al. (1991) indicated the importance of the liquid charge, the contact angle and the shear stresses at the liquid–vapor interface in predicting the maximum heat-transfer capacity and thermal resistance of these devices.

Ma et al. (1996) developed a closed mathematical model of the liquid friction factor for flow occurring in triangular grooves. This model, which built upon the earlier work of Ma et al. (1994), considered the

interfacial shear stresses due to liquid–vapor frictional interactions for countercurrent flow. Using a coordinate transformation and the Nachtsheim–Swigert iteration scheme, the importance of the liquid–vapor interactions on the operational characteristics of micro heat pipes and other small phase-change devices was demonstrated. The solution resulted in a method by which the velocity distribution for countercurrent liquid–vapor flow could be determined and allowed the governing liquid flow equations to be solved for cases where the liquid surface is strongly influenced by the vapor flow direction and velocity. The results of the analysis were verified using an experimental test facility constructed with channel angles of 20, 40 and 60 degrees. The experimental and predicted results were compared and found to be in good agreement [Ma and Peterson 1996a; 1996b; Peterson and Ma, 1996a].

31.2.2 Testing of Individual Micro Heat Pipes

As fabrication capabilities have developed, experimental investigations on individual micro heat pipes have been conducted on progressively smaller and smaller devices, beginning with early investigations on what now appear to be relatively large micro heat pipes, approximately 3 mm in diameter, and progressing to micro heat pipes in the 30- μm -diameter range. These investigations have included both steady-state and transient investigations.

31.2.2.1 Steady-State Experimental Investigations

In the earliest experimental tests of this type reported in the open literature by Babin et al. (1990), several micro heat pipes approximately 1 mm in external diameter were evaluated. The primary purpose of this investigation was to determine the accuracy of the previously described steady-state modeling techniques, to verify the micro heat pipe concept, and to determine the maximum heat-transport capacity. The fabrication techniques used to produce these test articles were developed by Itoh Research and Development Company, Osaka, Japan [Itoh, 1988]. As reported previously, four test articles were evaluated, two each from silver and copper. Two of these test pipes were charged with distilled, deionized water and the other two were used in an uncharged condition to determine the effect of the vaporization–condensation process on the overall thermal conductivity of these devices. Steady-state tests were conducted over a range of tilt angles to determine the effect of the gravitational body force on the operational characteristics. An electrical resistance heater supplied the heat into the evaporator. Heat rejection was achieved through the use of a constant-temperature ethyl–glycol solution, which flowed over the condenser portion of the heat pipe. The axial temperature profile was continuously monitored by five thermocouples bonded to the outer surface of the heat pipe using a thermally conductive epoxy. Three thermocouples were located on the evaporator: one on the condenser and one on the outer surface of the adiabatic section. Throughout the tests, the heat input was systematically increased and the temperature of the coolant bath adjusted to maintain a constant adiabatic wall temperature [Babin et al., 1990].

The results of this experiment have been utilized as a basis for comparison with a large number of heat pipe models. As previously reported [Peterson et al., 1996], the steady-state model of Babin et al. (1990) overpredicted the experimentally determined heat-transport capacity at operating temperatures below 40°C and underpredicted it at operating temperatures above 60°C. These experimental results represented the first successful operation of a “micro” heat pipe that utilized the principles outlined in the original concept of Cotter (1984) and as such paved the way for numerous other investigations and applications.

31.2.2.2 Transient Experimental Investigations

While the model developed by Babin et al. (1990) was shown to predict the steady-state performance limitations and operational characteristics of the trapezoidal heat pipe reasonably well for operating temperatures between 40 and 60°C, little was known about the transient behavior of these devices. As a result, Wu et al. (1991) undertook an experimental investigation of the transient characteristics of these devices. This experimental investigation again utilized micro heat pipe test articles developed by Itoh (1988); however, this particular test pipe was designed to fit securely under a ceramic chip carrier and

had small fins at the condenser end of the heat pipe for removal of heat by free or forced convection, as shown in [Figure 31.1](#). Startup and transient tests were conducted in which the transient response characteristics of the heat pipe as a function of incremental power increases, tilt angle, and mean operating temperature were measured.

Itoh and Polásek (1990a; 1990b) presented the results of an extensive experimental investigation on a series of micro heat pipes ranging in size and shape from 1 to 3 mm in diameter and 30 to 150 mm in length that utilized both cross-sectional configurations, similar to those presented previously, and a conventional internal wicking structure (Polásek, 1990; Fejfar et al., 1990). The unique aspect of this particular investigation was the use of neutron radiography to determine the distribution of the working fluid within the heat pipes [Itoh and Polásek, 1990a; 1990b; Ikeda, 1990]. Using this technique, the amount and distribution of the working fluid and noncondensable gases were observed during real-time operation along with the boiling and/or re-flux flow behavior. The results of these tests indicated several important results [Peterson, 1992]:

- As is the case for conventional heat pipes, the maximum heat-transport capacity is principally dependent upon the mean adiabatic vapor temperature.
- Micro heat pipes with smooth inner surfaces were found to be more sensitive to overheating than those with grooved capillary systems.
- The wall thickness of the individual micro heat pipes had a greater effect on the thermal performance than did the casing material.
- The maximum transport capacity of heat pipes utilizing axial channels for return of the liquid to the evaporator was found to be superior to that of those utilizing a formal wicking structure.

31.3 Arrays of Micro Heat Pipes

31.3.1 Modeling of Heat Pipe Arrays

The initial conceptualization of micro heat pipes by Cotter (1984) envisioned fabricating micro heat pipes directly into semiconductor devices as shown schematically in [Figure 31.3](#). While many of the previously discussed models can be used to predict the performance limitations and operational characteristics of individual micro heat pipes, it is not clear from the models or analyses how the incorporation of an array of these devices might affect the temperature distribution or the resulting thermal performance. Mallik et al. (1991) developed a three-dimensional numerical model capable of predicting the thermal performance of an array of parallel micro heat pipes constructed as an integral part of semiconductor chips, similar to that illustrated in [Figure 31.4](#). In order to determine the potential advantages of this concept, several different thermal loading configurations were modeled, and reduction in maximum surface temperature, the mean chip temperature and the maximum temperature gradient across the chip was determined [Peterson, 1994].

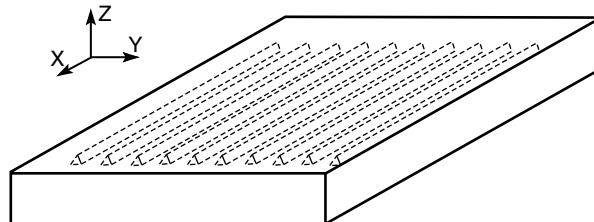


FIGURE 31.3 Array of micro heat pipes fabricated as an integral part of a silicon wafer.

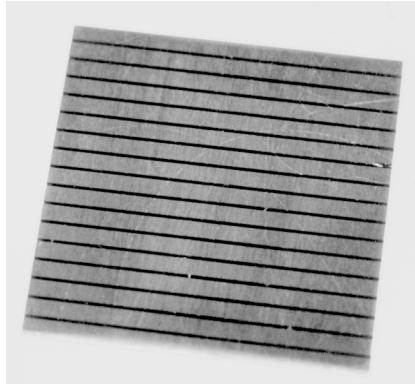


FIGURE 31.4 Silicon wafer into which an array of micro heat pipes has been fabricated.

Although the previous investigations of Babin et al. (1990), Wu and Peterson (1991) and Wu et al. (1991) indicated that an effective thermal conductivity greater than 10 times that of silicon could be achieved, additional analyses were conducted to determine the effect of variations in this value. Steady-state analyses were performed using a heat pipe array comprised of 19 parallel heat pipes. Using an effective thermal conductivity ratio of 5, the maximum and mean surface temperatures were 37.69 and 4.91°C, respectively. With an effective thermal conductivity ratio of 10, the maximum and mean surface temperatures were 35.20 and 4.21°C, respectively. Using an effective thermal conductivity ratio of 15, the maximum and mean surface temperatures were 32.67 and 3.64°C, respectively [Peterson, 1994]. These results illustrate how the incorporation of an array of micro heat pipes can reduce the maximum wafer temperature, reduce the temperature gradient across the wafers and eliminate localized hot spots. In addition, this work highlighted the significance of incorporating these devices into semiconductor chips, particularly those constructed in materials with thermal conductivities significantly less than that of silicon, such as gallium arsenide.

This work was further extended to determine transient response characteristics of an array of micro heat pipes fabricated into silicon wafers as a substitute for polycrystalline diamond or other highly thermally conductive heat spreader materials [Mallik and Peterson, 1991; Mallik et al., 1992]. The resulting transient, three-dimensional, numerical model was capable of predicting the time-dependent temperature distribution occurring within the wafer when given the physical parameters of the wafer and the locations of the heat sources and sinks and indicated that significant reductions in the maximum localized wafer temperatures and thermal gradients across the wafer could be obtained through the incorporation of an array of micro heat pipes. Utilizing heat sinks located on the edges of the chip perpendicular to the axis of the heat pipes and a cross-sectional area porosity of 1.85%, reductions in the maximum chip temperature of up to 40% were predicted.

31.3.2 Testing of Arrays of Micro Heat Pipes

Peterson et al. (1991) fabricated, charged and tested micro heat pipe arrays incorporated as an integral part of semiconductor wafers. These tests represented the first successful operation of these devices reported in the open literature. In this investigation, several silicon wafers were fabricated with distributed heat sources on one side and an array of micro heat pipes on the other, as illustrated in Figure 31.4. Since that time, a number of experimental investigations have been conducted to verify the micro heat pipe array concept and determine the potential advantages of constructing an array of micro heat pipes as an integral part of semiconductor devices [Peterson et al., 1993; Peterson, 1994]. The arrays tested have typically been fabricated in silicon and have ranged in size from parallel rectangular channels, 30 μm wide, 80 μm deep and 19.75 mm long, machined into a silicon wafer 20 mm square and 0.378 mm thick with an interchannel spacing of 500 μm , to etched arrays of triangular channels, 120 μm wide and 80 μm

CONSTRUCTION PROCESS

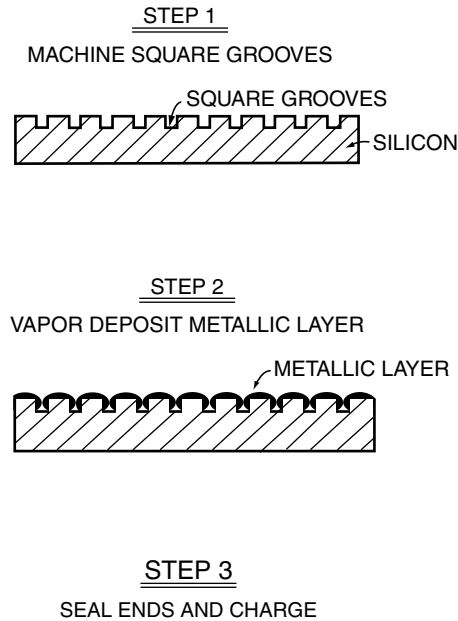


FIGURE 31.5 Vapor deposition process for fabricating micro heat pipes.

deep machined into 20-mm-square silicon wafers 0.5 mm thick [Peterson et al., 1993]. In addition, arrays of micro heat pipes fabricated using a vapor deposition process first proposed by Peterson (1990) and illustrated in Figure 31.5 were tested by Mallik et al. (1995).

In this work, wafers with arrays of 34 and 66 micro heat pipes were evaluated using an infrared thermal imaging system in conjunction with a VHS video recorder. These arrays occupied 0.75% and 1.45% of the wafer cross-sectional area, respectively. The wafers with micro heat pipe arrays demonstrated a 30 to 45% reduction in the thermal time constant when compared to that obtained for plain silicon wafers, which led to a significant reduction in the maximum wafer temperature. The experimental results were then used to validate the transient numerical model described previously [Peterson and Mallik, 1995].

31.3.3 Fabrication of Arrays of Micro Heat Pipes

Considerable information is available on the methods used to fabricate micro heat pipes with hydraulic diameters on the order of 20 to 150 μm into silicon or gallium arsenide wafers. These early investigations included the use of conventional techniques such as the machining of small channels [Peterson, 1988b; Peterson et al., 1991], the use of directionally dependent etching processes to create rectangular- or triangular-shaped channels [Peterson, 1988b; Gerner, 1990; Mallik et al., 1991; Gerner et al., 1992] or other more elaborate techniques that utilize the multisource vapor deposition process illustrated in Figure 31.5 [Mallik et al., 1991; Weichold et al., 1993] to create an array of long, narrow channels of triangular cross section lined with a thin layer of copper. Peterson (1994) has summarized these. The earliest fabricated arrays were machined into a silicon wafer 2 cm square and 0.378 mm thick, with an inter-channel spacing of 500 μm . Somewhat later, Adkins et al. (1994) reported on a different fabrication process used for an array of heat pipes with a segmented vapor space. Peterson (1988b), Gerner (1990), Peterson et al. (1993), Ramadas et al. (1993) and Gerner et al. (1994) have described other processes. All of these techniques are similar in nature and typically utilize conventional photolithography masking techniques, coupled with an orientation-dependent etching technique.

Perhaps the most important aspects of these devices are the shape and relative areas of the liquid and vapor passages. A number of investigations have been directed at the optimization of these grooves. These include investigations by Ha and Peterson (1994) that analytically evaluated the axial dryout of the evaporating thin liquid film, one by Ha and Peterson (1996) that evaluated the interline heat transfer and others that examined other important aspects of the problem. [Ha and Peterson, 1998a; 1998b; Peterson and Ha, 1998; Ma and Peterson, 1998]. These studies and others have shown both individual and arrays of micro heat pipes to be extremely sensitive to flooding [Peterson, 1992], and for this reason several different charging methods have been developed and described in detail [Duncan and Peterson, 1995]. These vary from those that are similar to the methods utilized on larger more conventional heat pipes to a method in which the working fluid is added and then the wafer is heated to above the critical temperature of the working fluid so that the working fluid is in the supercritical state and exists entirely as a vapor. The array is then sealed and allowed to cool to below the critical temperature, allowing the vapor to cool and condense. Because, when in the critical state, the working fluid is uniformly distributed throughout the individual micro heat pipes, the exact charge can be carefully controlled and calculated.

31.4 Flat-Plate Micro Heat Spreaders

While arrays of micro heat pipes have the ability to significantly improve the effective thermal conductivity of silicon wafers and other conventional heat spreaders, they are of limited value in that they only provide heat transfer along the axial direction of the individual heat pipes. To overcome this problem, flat-plate heat spreaders, capable of distributing heat over a large two-dimensional surface have been proposed by Peterson (1992; 1994). In this application, a wicking structure is fabricated in silicon multichip module substrates to promote distribution of the fluid and vaporization of the working fluid (Figure 31.6). This wick structure is the key element in these devices and several methods for wick manufacture have been considered [Peterson et al. 1996].

In the most comprehensive investigation of these devices to date, a flat-plate micro heat pipe similar to that described by Peterson et al. (1996) was fabricated in silicon multichip module substrates 5 mm × 5 mm square [Benson et al., 1996a; 1996b]. These devices, which are illustrated in Figure 31.6, utilized two separate silicon wafers. On one of the two wafers, the wick pattern was fabricated leaving a small region around the perimeter of the wafer unpatterned to allow the package to be hermetically sealed. The other silicon wafer was etched in such a manner that a shallow well was formed that corresponded to the wick area. The two pieces were then wafer-bonded together along the seal ring. Upon completion

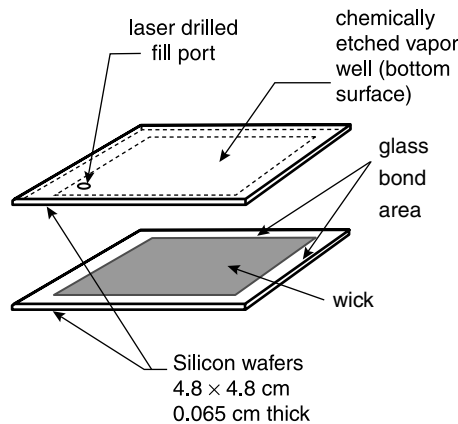


FIGURE 31.6 Flat-plate micro heat spreader. (From Benson, D.A. et al. (1996a) *Proc. IEEE Multichip Module Conf.*, Santa Clara, CA. © 1996 IEEE. With permission.)

of the fabrication, the flat-plate micro heat pipe was filled through a small laser-drilled port located in one corner of the wafer. Because the entire wicking area was interconnected, the volume of the liquid required to charge was of sufficient volume that conventional charging techniques could be utilized [Benson et al., 1996b].

31.4.1 Modeling of Micro Heat Spreaders

Analytical investigations of the performance of these micro heat spreaders or flat-plate heat pipes have been underway for some time; Benson et al. (1996a; 1996b) and Peterson (1996) have summarized the results. These investigations have demonstrated that these devices can provide an effective mechanism for distributing the thermal load in semiconductor devices and reducing the localized hot spots resulting from active chip sites [Peterson, 1996]. The models indicate that the performance of these devices is excellent. In addition, because these devices can be made from silicon, Kovar or a wide variety of other materials, an excellent match between the coefficient of thermal expansion (CTE) can be achieved, while keeping the material and fabrication costs very low. A number of different wicking structures have been considered. Among these are wicks fabricated using a silicon dicing saw (Figure 31.7), wicks fabricated using conventional anisotropic etching techniques (Figure 31.8) and wicks fabricated using a deep plasma etching technique (Figure 31.9). Recent modeling has focused on the development of optimized wicking structures that could be fabricated directly into the wafer and provide maximum capillary pumping while optimizing the thin-film region of the meniscus in order to maximize the heat flux [Wayner et al., 1976; Peterson and Ma, 1996b; 1999].

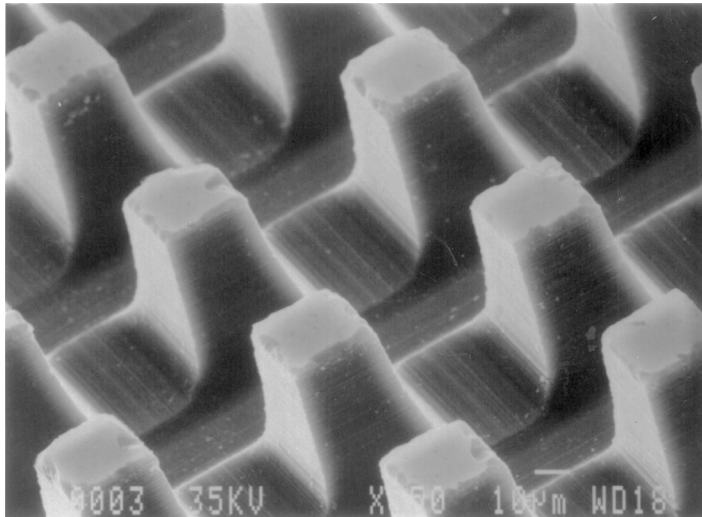


FIGURE 31.7 Wick pattern prepared with bidirectional saw cuts on a silicon wafer. (From Benson, D.A. et al. (1996b) *Advances in Design, Materials and Processes for Thermal Spreaders and Heat Sinks Workshop*, April 19–21, Vail, CO. © 1996 IEEE. With permission.)



FIGURE 31.8 Chemically etched orthogonal, triangular groove wick. (From Mallik, A.K., and Peterson, G.P. (1991) in *3rd ASME–JSME Thermal Engineering Joint Conf. Proc.*, Vol. 2, March 17–22, Reno, NV, pp. 394–401. With permission.)

TABLE 31.1 Thermal Conductivity, Coefficient of Thermal Expansion, Cost Estimates and Scaling Trends of Current and Potential Substrate Materials

Materials	Thermal Conductivity (W/cm-K)	Coefficient of Thermal Expansion ($10^{-6}/K$)	Cost of Substrate (\$/in ²)	Scaling with Area Cost Trend
Alumina	0.25	6.7	0.09	6" limit
FR-4	Depends on copper	13.0	0.07	Constant to 36"
AlN	1.00–2.00	4.1	0.35	6" limit
Silicon	1.48	4.7	1.00	6–10" limit
Heat pipe in silicon	8.00 → 20.00 (?)	4.7	3.00	6–10" limit
Al	2.37	41.8	0.0009	Scales as area
Cu	3.98	28.7	0.0015	Scales as area
Diamond	10.00–20.00	1.0–1.5	1000.00	Scales as area ²
Kovar	0.13	5.0	0.027	Scales as area
Heat pipe in Kovar	>8.00	5.0	0.10	Scales as area
AlSiC	2.00 (at 70%)	7.0 (?)	1.00	Casting size limited

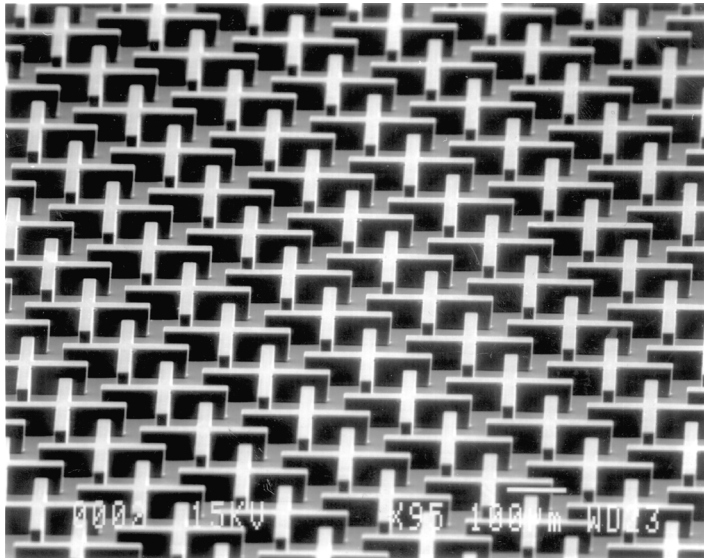


FIGURE 31.9 Wick pattern on silicon prepared by a photomask and deep plasma etch technique; 25- μm -wide \times 50- μm -deep wafer. (From Benson, D.A. et al. (1996b) *Advances in Design, Materials and Processes for Thermal Spreaders and Heat Sinks Workshop*, April 19–21, Vail, CO. © 1996 IEEE. With permission.)

The results of these optimization efforts have demonstrated that these microscale flat-plate heat spreaders allow the heat to be dissipated in any direction across the wafer surface, thereby vastly improving performance. The resulting effective thermal conductivities can approach and perhaps exceed those of diamond coatings of equivalent thicknesses. Table 31.1 [Benson et al., 1998] illustrates the relative comparison of these flat-plate heat pipes and other types of materials traditionally utilized in the electronics industry for heat spreading. In this comparison, it is important to note that the ideal heat spreader would have the thermal conductivity of diamond, a coefficient of thermal expansion of silicon, and a cost comparable to aluminum. As shown, flat-plate heat pipes fabricated in either silicon or Kovar compare very favorably with diamond in terms of thermal conductivity and have a coefficient of thermal expansion relatively close to silicon (or exactly, in the case of silicon), and a projected cost that is quite low. Based upon this comparison, it would appear that these flat-plate heat pipes have tremendous commercial potential.

31.4.2 Testing of Micro Heat Spreaders

As described by Benson et al. (1998), a number of different flat-plate micro heat pipe test articles have been evaluated using an infrared camera to determine the spatially resolved temperature distribution. Using this information and a technique initially described by Peterson (1993) for arrays of micro heat pipes, the effective thermal conductivities of charged and uncharged flat-plate micro heat pipes and a series of micro heat spreaders were evaluated experimentally. The results indicated that an effective thermal conductivity between 10 and 20 W/cm-K was possible over a fairly broad temperature range. These values of thermal conductivity approach those of polycrystalline diamond substrates, or are more than five times that of a solid silicon substrate even at elevated temperatures (50°C) and power levels (15 W/cm²). The cost of such advanced silicon substrates is estimated at \$.60/cm² (see Table 31.1). Any other inexpensive material with a CTE close to that of the chip may also be a potential option for the heat pipe case material. For example, many alloys in the Fe/Ni/Co family have CTEs closely matching those of semiconductor materials [Benson et al., 1996].

As noted by Peterson (1992), several aspects of the technology remain to be examined before flat-plate micro heat spreaders can come into widespread use, but it is clear from the results of these early experimental tests that spreaders such as the ones discussed here, fabricated as integral parts of silicon chips, present a feasible alternative cooling scheme that merits serious consideration for a number of heat-transfer applications.

31.4.3 Fabrication of Micro Heat Spreaders

The fabrication of these micro heat spreaders is basically just an extension of the methods used by several early investigations to fabricate individual micro heat pipes with hydraulic diameters on the order of 20 to 150 μm. As discussed previously, a number of different wicking structures have been utilized. These wicking structures have been Kovar, silicon or gallium arsenide and include the use of conventional techniques such as machining, directionally dependent etching and deep plasma etching multisource vapor deposition processes. Charging of these devices is somewhat easier than for the individual arrays of micro heat pipes and, while these devices are still sensitive to undercharge, they can accommodate an overcharge much more readily.

31.5 New Designs

In addition to the designs described above, several new designs are currently being developed and evaluated for use in conventional electronic applications and for advanced spacecraft applications. The function of these designs is to provide lightweight, flexible flat-plate heat pipes capable of collecting heat from high heat-flux sources and transporting it to large surface areas where it can be dissipated. In electronic applications, this may entail the collection of heat from a microprocessor and transport of it to a conventional heat spreader or to a more readily available heat sink, such as the screen of a laptop computer. In advanced spacecraft applications, these devices may be used to fabricate highly flexible radiator fin structures for use on long-term spacecraft missions.

To date, several new designs have been proposed. The first of these consists of a flexible, micro heat pipe array, fabricated by sintering an array of aluminum wires between two thin aluminum sheets as shown in Figure 31.10. In this design, the sharp corner regions formed by the junction of the plate and the wires act as the liquid arteries. When made of aluminum with ammonia or acetone as the working fluid, these devices become excellent candidates for use as flexible radiator panels for long-term spacecraft missions and can have a thermal conductivity that greatly exceeds the conductivity of an equivalent thickness of any known material.

A numerical model, combining both conduction and radiation effects, has been developed to predict the heat-transfer performance and temperature distribution of these types of radiator fins in a simulated space environment [Wang et al., 2000]. Three different configurations were analyzed and experimentally

TABLE 31.2 Configurations of Microheat Pipes

	Prototype		
	No. 1	No. 2	No. 3
Material	Aluminum	Aluminum	Aluminum
Working fluid	Acetone	Acetone	Acetone
Total dimension (mm)	152 × 152.4	152 × 152.4	152 × 152.4
Thickness of sheet (mm)	0.40	0.40	0.40
Diameter of wire (mm)	0.50	0.80	0.50
Number of wires	43	43	95

Source: From Wang, Y. et al. (2000) Paper No. AIAA-2000-0969, 38th Aerospace Sciences Meeting, January 10–13, Reno, NV. With permission.

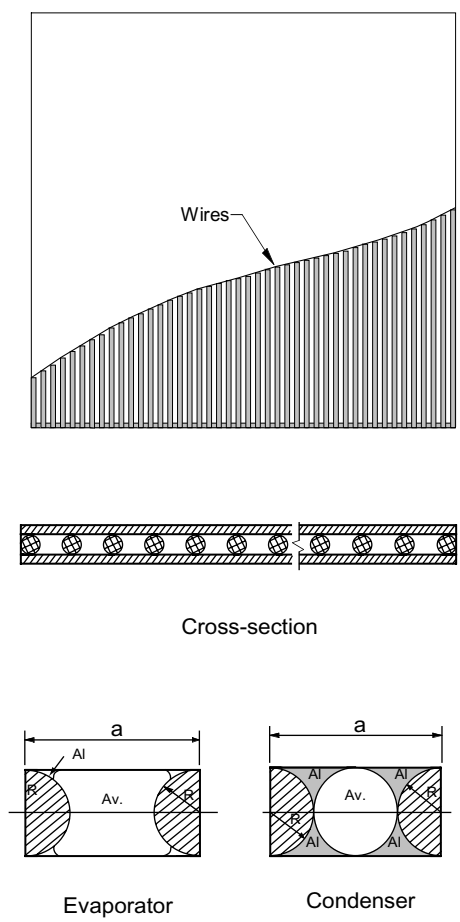


FIGURE 31.10 Flexible wire bonded heat pipe. (From Wang, Y. et al. (2000) Paper No. AIAA-2000-0696, 38th Aerospace Sciences Meeting, January 10–13, Reno, NV. With permission.)

evaluated, and the results were compared. Each of the three configurations was modeled both with and without a working fluid charge in order to determine the reduction in the maximum temperature, mean temperature and temperature gradient on the radiator surface. Table 31.2 lists the physical specifications of the three micro heat pipe arrays fabricated. Acetone was used as the working fluid in both the modeling effort and also in the actual experimental tests.

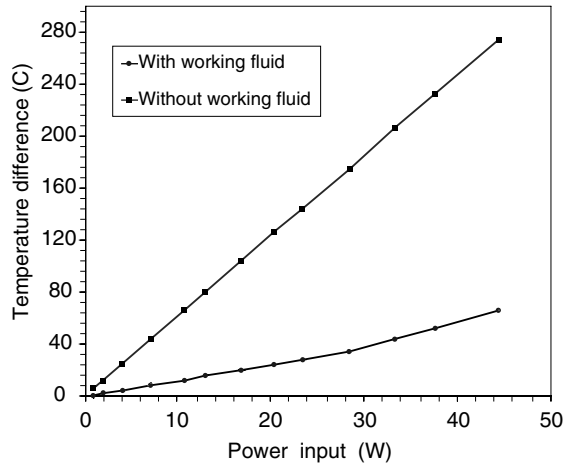


FIGURE 31.11 Temperature difference of micro heat pipe arrays with or without working fluid. (From Wang, Y. et al. (2000) Paper No. AIAA-2000-0696, 38th Aerospace Sciences Meeting, January 10–13, Reno, NV. With permission.)

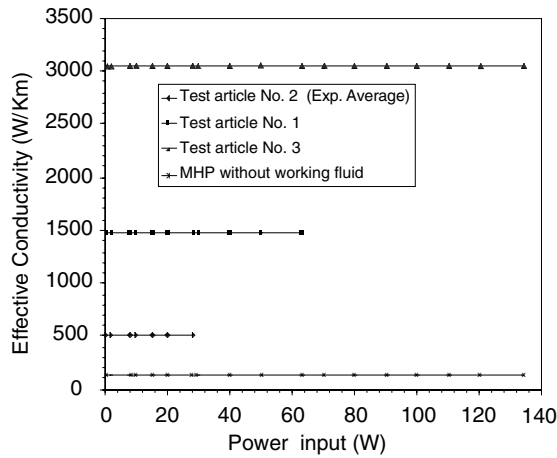


FIGURE 31.12 Effective thermal conductivity of micro heat pipe arrays. (From Wang, Y. et al. (2000) Paper No. AIAA-2000-0696, 38th Aerospace Sciences Meeting, January 10–13, Reno, NV. With permission.)

The results of the preliminary tests conducted on these configurations are shown in [Figure 31.11](#). As indicated, the heat transport was proportional to the temperature difference between the evaporator and condenser; i.e., the effective thermal conductivity of the micro heat pipe array was constant with respect to the temperature. From the temperature difference and heat transport obtained as shown in [Figure 31.11](#) the effective conductivity was obtained. As illustrated in [Figure 31.12](#), the effective thermal conductivities of micro heat pipe arrays No.1, 2 and 3 were 1446.2, 521.3 and 3023.1 W/Km, respectively. For the micro heat pipe arrays without any working fluid, the effective conductivities in the x -direction were 126.3, 113.0 and 136.2 W/Km, respectively. Comparison of the predicted and experimental results indicated that these flexible radiators, with the arrays of micro heat pipes, have an effective thermal conductivity between 15 and 20 times that of the uncharged version. This results in a more uniform temperature distribution, which could significantly improve the overall radiation effectiveness, reduce the overall size, and meet or exceed the baseline design requirements for long-term manned missions to Mars.

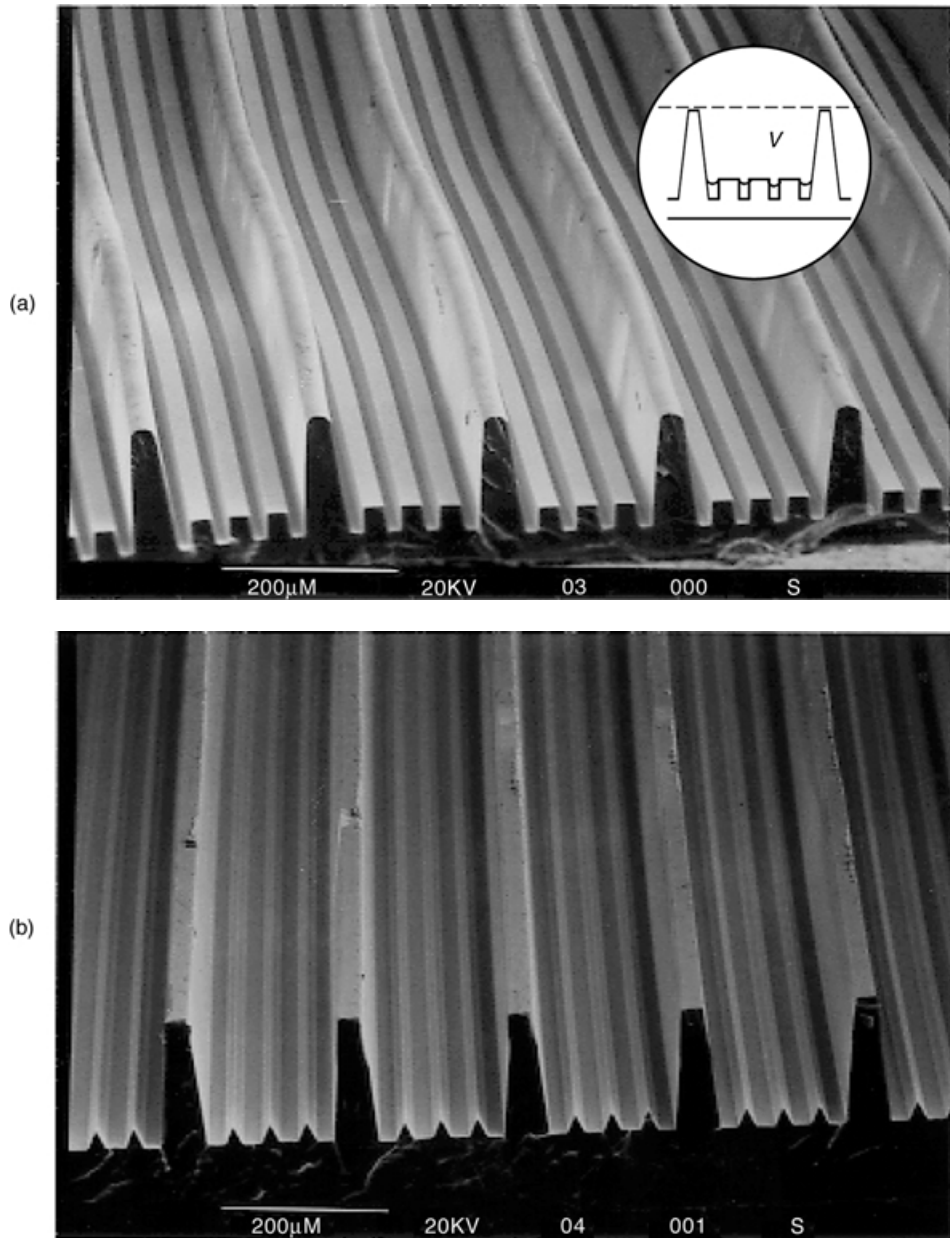


FIGURE 31.13 Flexible polymer micro heat pipe. (a) Rectangular grooves; (b) trapezoidal grooves.

The second design currently being considered consists of an array of flexible micro heat pipes fabricated in a polymer material, as illustrated in Figure 31.13a. This material is extruded in such a fashion that it has a series of large rectangular grooves that serve as the actual heat pipes, each approximately 200 μm wide. Within each of these micro heat pipes is a series of smaller grooves that serve as the liquid arteries (see inset). As shown in Figure 31.13a, these grooves can be rectangular in nature or, as shown in Figure 31.13b, they can be trapezoidal. In both cases, the material is polypropylene, and the internal dimension of the individual heat pipes is approximately 200 μm . The smaller grooves within each of the individual heat pipes are designed to transport the fluid from the evaporator to the condenser. While only preliminary

experimental test data are available, this design appears to hold great promise for both spacecraft radiator applications and also for flexible heat spreaders for use in Earth-based electronic applications.

31.6 Summary and Conclusions

It is clear from the preceding review that the concept of using microscale heat pipes and/or flat-plate micro heat spreaders is feasible, practical and cost effective. A number of different concepts and sizes have been shown to be acceptable from both an experimental and theoretical perspective, and a number of these devices are already in widespread use. Steady-state and transient models have been developed and verified experimentally and are capable of predicting the operational limits and performance characteristics of micro heat pipes with diameters less than 100 microns with a high degree of reliability. These models are currently being expanded for use in both individual heat pipes and also with arrays of heat pipes constructed as an integral part of semiconductor devices.

In addition to the analytical work, experimental evaluation has indicated that these devices can be effective in dissipating and transporting heat from localized heat sources and are presently being used in a number of commercial applications. Arrays of micro heat pipes on the order of 35 microns have been successfully fabricated, charged and tested, and incorporated as an integral part of semiconductor devices. Extensive testing has indicated that these heat pipes can provide an effective method for dissipating localized heat fluxes, eliminating localized hot spots, reducing the maximum wafer temperatures and thereby improving the wafer reliability.

Finally, several new designs have been and continue to be developed that have applications ranging from spacecraft radiator applications to land-based electronics applications. These new designs incorporate optimized wicking structures and clever new fabrication schemes, along with materials not previously utilized for heat pipe applications.

Nomenclature

- A = area (m^2)
- C = constant (defined in text)
- d = diameter (m)
- f = drag coefficient (dimensionless)
- k = thermal conductivity (W/m-K)
- K = wick permeability (m^2)
- L = length (m)
- Ma = Mach number (dimensionless)
- P = pressure (N/m^2)
- q = heat flow rate (W)
- R = thermal resistance (K/W) or universal gas constant (J/kg-K)
- Re = Reynolds number (dimensionless)
- r = radius (m)
- T = temperature (K)
- V = velocity (m/s)
- w = groove width (m) or wire spacing (m)
- We = Weber number (dimensionless)

Greek Symbols

- λ = latent heat of vaporization (J/kg)
- μ = dynamic viscosity (kg/m-s)
- ρ = density (kg/m^3)

σ = surface tension (N/m)
 τ = shear stress (N/m²)
 Ψ = angle of inclination (degrees or radians)

Subscripts

b = boiling
 c = capillary, capillary limitation, condenser
 e = entrainment, evaporator section
 eff = effective
 f = fin
 h = hydraulic
 i = inner
 l = liquid
 m = maximum
 o = outer
 p = pipe
 s = sonic
 v = vapor
 w = wire spacing, wick
– = axial hydrostatic pressure
+ = normal hydrostatic pressure

References

- Adkins, D.R., Shen, D.S., Palmer, D.W., and Tuck, M.R., (1994) "Silicon Heat Pipes for Cooling Electronics," in *Proc. 1st Annu. Spacecraft Thermal Control Symp.*, November 16–18, Albuquerque, NM.
- Anon. (1989) "Application of Micro Heat Pipes in Hyperthermia," Annual Report of the Itoh Research and Development Laboratory, Osaka, Japan.
- Babin, B.R., and Peterson, G.P. (1990) "Experimental Investigation of a Flexible Bellows Heat Pipe for Cooling Discrete Heat Sources," *ASME J. Heat Transfer* **112**(3), pp. 602–607.
- Babin, B.R., Peterson, G.P., and Wu, D. (1990) "Steady-State Modeling and Testing of a Micro Heat Pipe," *ASME J. Heat Transfer* **112**(3), pp. 595–601.
- Badran, B., Gerner, F.M., Ramadas, P., Henderson, H.T., and Baker, K.W. (1993) "Liquid Metal Micro Heat Pipes," 29th National Heat Transfer Conference, Atlanta, CA, *HTD*, **236**, pp. 71–85.
- Benson, D.A., Mitchell, R.T., Tuck, M.R., Adkins, D.R., and Palmer, D.W. (1996a) "Micro-Machined Heat Pipes in Silicon MCM Substrates," in *Proc. IEEE Multichip Module Conf.*, Santa Clara, CA.
- Benson, D.A., Adkins, D.R., Peterson, G.P., Mitchell, R.T., Tuck, M.R., and Palmer, D.W. (1996b) "Turning Silicon Substrates into Diamond: Micromachining Heat Pipes," in *Advances in Design, Materials and Processes for Thermal Spreaders and Heat Sinks Workshop*, April 19–21, Vail, CO.
- Benson, D.A., Adkins, D.R., Mitchell, R.T., Tuck, M.R., Palmer, D.W., and Peterson, G.P. (1998) "Ultra High Capacity Micro Machined Heat Spreaders," *Microscale Thermophys. Eng.* **2**(1), pp. 21–29.
- Camarda, C.J., Rummeler, D.R., and Peterson, G.P. (1997) "Multi Heat Pipe Panels," *NASA Technical Briefs*, LAR-14150.
- Chi, S.W. (1976) *Heat Pipe Theory and Practice*, McGraw-Hill, New York.
- Collier, J.G. (1981) *Convective Boiling and Condensation*, McGraw-Hill, New York.
- Colwell, G.T., and Chang, W.S. (1984) "Measurements of the Transient Behavior of a Capillary Structure under Heavy Thermal Loading," *Int. J. Heat Mass Transfer* **27**(4), pp. 541–551.
- Cotter, T.P. (1984) "Principles and Prospects of Micro Heat Pipes," in *Proc. 5th Int. Heat Pipe Conf.*, Tsukuba, Japan, pp. 328–335.
- Duncan, A.B., and Peterson, G.P. (1995) "Charge Optimization of Triangular Shaped Micro Heat Pipes," *AIAA J. Thermophys. Heat Transfer* **9**(2), pp. 365–367.

- Dunn, P.D., and Reay, D.A. (1982) *Heat Pipes*, 3rd ed., Pergamon Press, New York.
- Fejfar, K., Polásek, F., and Stulc, P. (1990) "Tests of Micro Heat Pipes," Annual Report of the SVÚSS, Prague.
- Fletcher, L.S., and Peterson, G.P. (1993) "A Micro Heat Pipe Catheter for Local Tumor Hyperthermia," U.S. Patent 5,190,539.
- Gaugler, R.S. (1944) "Heat Transfer Devices," U.S. Patent 2,350,348.
- Gerner, F.M. (1990) "Micro Heat Pipes," AFSOR Final Report No. S-210-10MG-066, Wright-Patterson AFB, Dayton, OH.
- Gerner, F.M., Longtin, J.P., Ramadas, P., Henderson, T.H., and Chang, W.S. (1992) "Flow and Heat Transfer Limitations in Micro Heat Pipes," in *28th National Heat Transfer Conf.*, August 9–12, San Diego, CA.
- Gerner, F.M., Badran, B., Henderson, H.T., and Ramadas, P. (1994) "Silicon-Water Micro Heat Pipes," *Thermal Sci. Eng.* **2**(1), pp. 90–97.
- Ha, J.M., and Peterson, G.P. (1994) "Analytical Prediction of the Axial Dryout of an Evaporating Liquid Film in Triangular Micro Channels," *ASME J. Heat Transfer* **116**(2), pp. 498–503.
- Ha, J.M., and Peterson, G.P. (1996) "The Interline Heat Transfer of Evaporating Thin Films along a Micro Grooved Surface," *ASME J. Heat Transfer* **118**(4), pp. 747–755.
- Ha, J.M., and Peterson, G.P. (1998a) "Capillary Performance of Evaporating Flow in Micro Grooves: An Analytical Approach for Very Small Tilt Angles," *ASME J. Heat Transfer* **120**(2), pp. 452–457.
- Ha, J.M., and Peterson, G.P. (1998b) "The Maximum Heat Transport Capacity of Micro Heat Pipes," *ASME J. Heat Transfer* **120**(4), pp. 1064–1071.
- Ikeda Y. (1990) "Neutron Radiography Tests of Itoh's Micro Heat Pipes," private communication, Nagoya University to F. Polásek.
- Itoh, A. (1988) *Micro Heat Pipes*, Prospectus of the Itoh R and D Laboratory, Osaka, Japan.
- Itoh, A., and Polásek, F. (1990a) "Development and Application of Micro Heat Pipes," in *Proc. 7th Int. Heat Pipe Conf.*, May 21–25, Minsk, USSR.
- Itoh, A., and Polásek, F. (1990b) "Micro Heat Pipes and Their Application in Industry," in *Proc. Czechoslovak-Japanese Symp. on Heat Pipes*, Rícany, Czechoslovakia.
- Kendall, D.L. (1979) "Vertical Etching of Silicon at Very High Aspect Ratios," *Ann. Rev. Mater. Sci.*, **7**, pp. 373–403.
- Khrustalev, D., and Faghri, A. (1994) "Thermal Analysis of a Micro Heat Pipe" *ASME J. Heat Transfer* **116**(1), 189–198.
- Kraus, A.D., and BarCohen, A. (1983) *Thermal Analysis and Control of Electronic Equipment*, McGraw-Hill, New York.
- Longtin, J.P., Badran, B., and Gerner, F.M. (1994) "A One-Dimensional Model of a Micro Heat Pipe during Steady-State Operation," *ASME J. Heat Transfer* **116**, pp. 709–715.
- Ma, H.B., and Peterson, G.P. (1996a) "Experimental Investigation of the Maximum Heat Transport in Triangular Grooves," *ASME J. Heat Transfer* **118**(4), pp. 740–746.
- Ma, H.B., and Peterson, G.P. (1996b) "Temperature Variation and Heat Transfer in Triangular Grooves with an Evaporating Film," *AIAA J. Thermophys. Heat Transfer* **11**(1), pp. 90–98.
- Ma, H.B., and Peterson, G.P. (1998) "Disjoining Pressure Effect on the Wetting Characteristics in a Capillary Tube," *Microscale Thermophys. Eng.* **2**(4), pp. 283–297.
- Ma, H.B., Peterson, G.P., and Lu, X.J. (1994) "The Influence of the Vapor-Liquid Interactions on the Liquid Pressure Drop in Triangular Microgrooves," *Int. J. Heat Mass Transfer* **37**(15), pp. 2211–2219.
- Ma, H.B., Peterson, G.P., and Peng, X.F. (1996) "Experimental Investigation of Countercurrent Liquid-Vapor Interactions and Its Effect on the Friction Factor," *Exp. Thermal Fluid Sci.* **12**(1), pp. 25–32.
- Mallik, A.K., and Peterson, G.P. (1991) "On the Use of Micro Heat Pipes as an Integral Part of Semiconductors," in *3rd ASME-JSME Thermal Engineering Joint Conf. Proc.*, Vol. 2, March 17–22, Reno, NV, pp. 394–401.
- Mallik, A.K., and Peterson, G.P. (1995) "Steady-State Investigation of Vapor Deposited Micro Heat Pipe Arrays," *ASME J. Electronic Packaging* **117**(1), pp. 75–81.

- Mallik, A.K., Peterson, G.P., and Weichold, W. (1991) "Construction Processes for Vapor Deposited Micro Heat Pipes," in *10th Symp. on Electronic Materials Processing and Characteristics*, June 3–4, Richardson, TX.
- Mallik, A.K., Peterson, G.P., and Weichold, M.H. (1992) "On the Use of Micro Heat Pipes as an Integral Part of Semiconductor Devices," *ASME J. Electronic Packaging* **114**(4), pp. 436–442.
- Mallik, A.K., Peterson, G.P., and Weichold, M.H. (1995) "Fabrication of Vapor Deposited Micro Heat Pipes Arrays as an Integral Part of Semiconductor Devices," *ASME J. MEMS* **4**(3), pp. 119–131.
- Marto, P.J., and Peterson, G.P. (1988) "Application of Heat Pipes to Electronics Cooling," in *Advances in Thermal Modeling of Electronic Components and Systems* (A. Bar-Cohen and A.D. Kraus, Eds.), pp. 283–336. Hemisphere Publishing, New York.
- Mráček, P. (1988) "Application of Micro Heat Pipes to laser Diode Cooling," Annual Report of the VÚMS, Prague, Czechoslovakia.
- Peterson, G.P. (1987a) "Analysis of a Heat Pipe Thermal Switch," in *Proc. 6th Int. Heat Pipe Conf.*, Vol. 1, May 25–28, Grenoble, France, pp. 177–183.
- Peterson, G.P. (1987b) "Heat Removal Key to Shrinking Avionics," *Aerospace Am.* **8**(10), pp. 20–22.
- Peterson, G.P. (1988a) "Investigation of Miniature Heat Pipes," Final Report, Wright Patterson AFB, Contract No. F33615-86-C-2733, Task 9.
- Peterson, G.P. (1988b) "Heat Pipes in the Thermal Control of Electronic Components," invited paper, *Proc. 3rd Int. Heat Pipe Symp.*, September 12–14, Tsukuba, Japan, pp. 2–12.
- Peterson, G.P. (1990) "Analytical and Experimental Investigation of Micro Heat Pipes," in *Proc. 7th Int. Heat Pipe Conf.*, Paper No. A-4, May 21–25, Minsk, USSR.
- Peterson, G.P. (1992) "An Overview of Micro Heat Pipe Research," *Appl. Mechanics Rev.* **45**(5), pp. 175–189.
- Peterson, G.P. (1993) "Operation and Applications of Microscopic Scale Heat Pipes," in *Encyclopedia of Science and Technology*, Vol. 20, pp. 197–200. McGraw-Hill, New York.
- Peterson, G.P. (1994) *An Introduction to Heat Pipes: Modeling, Testing and Applications*, John Wiley & Sons, New York.
- Peterson, G.P. (1996) "Modeling, Fabrication and Testing of Micro Heat Pipes: An Update," *Appl. Mechanics Rev.* **49**(10), pp. 175–183.
- Peterson, G.P., and Ha, J.M. (1998) "Capillary Performance of Evaporating Flow in Micro Grooves: Approximate Analytical Approach and Experimental Investigation," *ASME J. Heat Transfer* **120**(3), pp. 743–751.
- Peterson, G.P., and Ma, H.B. (1996a) "Analysis of Countercurrent Liquid-Vapor Interactions and the Effect on the Liquid Friction Factor," *Exp. Thermal Fluid Sci.* **12**(1), pp. 13–24.
- Peterson, G.P., and Ma, H.B. (1996b) "Theoretical Analysis of the Maximum Heat Transport in Triangular Grooves: A Study of Idealized Micro Heat Pipes," *ASME J. Heat Transfer* **118**(4), pp. 734–739.
- Peterson, G.P., and Ma, H.B. (1999) "Temperature Response and Heat Transfer in a Micro Heat Pipe," *ASME J. Heat Transfer* **121**(2), pp. 438–445.
- Peterson, G.P., and Mallik, A.K. (1995) "Transient Response Characteristics of Vapor Deposited Micro Heat Pipe Arrays," *ASME J. Electronic Packaging* **117**(1), pp. 82–87.
- Peterson, G.P., and Ortega, A. (1990) "Thermal Control of Electronic Equipment and Devices," in *Advances in Heat Transfer*, Vol. 20 (J. P. Hartnett and T. F. Irvine, Eds.), pp. 181–314. Pergamon Press, New York.
- Peterson, G.P., Duncan, A.B., Ahmed, A.K., Mallik, A.K., and Weichold, M.H. (1991) "Experimental Investigation of Micro Heat Pipes in Silicon Devices," in *1991 ASME Winter Ann. Meeting*, ASME Vol. DSC-32, December 1–6, Atlanta, GA, pp. 341–348.
- Peterson, G.P., Duncan, A.B., and Weichold, M.H. (1993) "Experimental Investigation of Micro Heat Pipes Fabricated in Silicon Wafers," *ASME J. Heat Transfer* **115**(3), pp. 751–756.
- Peterson, G.P., Swanson, L.W., and Gerner, F.M. (1996) "Micro Heat Pipes," in *Microscale Energy Transport* (C. L. Tien, A. Majumdar, and F. M. Gerner, Eds.), Taylor & Francis, Washington, D.C.
- Polásek, F. (1990) "Testing and Application of Itoh's Micro Heat Pipes," Annual Report of the SVÚSS, Prague, Czechoslovakia.

- Ramadas, P., Badran, B., Gerner, F.M., Henderson, T.H., and Baker, K.W. (1993) "Liquid Metal Micro Heat Pipes Incorporated in Waste-Heat Radiator Panels," in *Tenth Symp. on Space Power and Propulsion*, January 10–14, Albuquerque, NM.
- Tien, C.L., Chung, K.S., and Lui, C.P. (1979) "Flooding in Two-Phase Countercurrent Flows," EPRI NP-1283, U.S. Department of Energy, Washington, D.C.
- Wang, Y., Ma, H.B., and Peterson, G.P. (2000) "Investigation of the Temperature Distributions on Radiator Fins with Micro Heat Pipes," Paper No. AIAA-2000-0969, 38th Aerospace Sciences Meeting, January 10–13, Reno, NV.
- Wayner, Jr., P.C., Kao, Y.K., and LaCroix, L.V. (1976) "The Interline Heat-Transfer Coefficient of an Evaporating Wetting Film," *Int. J. Heat Mass Transfer* **19**(3), pp. 487–492.
- Weichold, M.H., Peterson, G.P., and Mallik, A. (1993) *Vapor Deposited Micro Heat Pipes*, U.S. Patent 5,179,043.
- Wu, D., and Peterson, G.P. (1991) "Investigation of the Transient Characteristics of a Micro Heat Pipe," *AIAA J. Thermophys. Heat Transfer* **5**(2), pp. 129–134.
- Wu, D., Peterson, G.P., and Chang, W.S. (1991) "Transient Experimental Investigation of Micro Heat Pipes," *AIAA J. Thermophys. Heat Transfer* **5**(4), pp. 539–545.